Acta Oceanol. Sin., 2025, Vol. 44, No. 2, P. 91–103
https://doi.org/10.1007/s13131-024-2422-8

A new fixed-depth suspension control algorithm for mobile marine seismometer and its testing results

Fei Hou[1, 2], Jiabiao Li[2*], Xinke Zhu[2], Weiwei Ding[2], Zhiteng Yu[2]

[1] Hubei Key Laboratory of Marine Geological Resources, China University of Geosciences, Wuhan 430074, China
[2] State Key Laboratory of Submarine Geoscience,Second Institute of Oceanography, Ministry of Natural Resources, Hangzhou 310012, China

Received 8 May 2024; accepted 6 December 2024

Abstract
A mobile marine seismometer (MMS) is a vertical underwater vehicle that detects ocean seismic waves. One of the critical operational requirements for an MMS is that it remains suspended at a desired depth. This article aimed to propose a fixed-depth suspension control for the MMS with a limited onboard energy supply. The research team established a kinematic model to analyze fluctuations in the vertical motion of the MMS and the delayed response of the system. We ascertained a direct one-to-one correlation between the displacement volume of the mobile ocean seismic instrument and the depth at which it reaches a state of neutral buoyancy (commonly referred to as the hover depth). A fixed-depth control algorithm was introduced, allowing a gradual approach to the necessary displacement volume to reach the desired suspension depth. The study optimized the boundary conditions to reduce unnecessary adjustments and mitigate the time delay caused by the instrument's inertia, thereby significantly minimizing energy consumption. This method does not require calculating the hydrodynamic parameters or transfer functions of the MMS, thereby considerably reducing the implementation complexity. In the three-month sea trial in the South China Sea, the seismic instrument was set to hover at 800 m, with a permissible fluctuation of ±100 m, operating on a seven-day cycle. The experimental results show that the seismic instrument has an average hover error of 34.6 m, with a vertical drift depth of 29.6 m per cycle, and the buoyancy adjustment system made six adjustments, indicating that our proposed control method performs satisfactorily. In addition, this method provides new insights for the fixed-depth control of other ocean observation devices that rely on buoyancy adjustment.

Key words mobile marine seismometer, fixed-depth control algorithm, low buoyancy-adjustment cost, faster convergence speed

Citation Hou Fei, Li Jiabiao, Zhu Xinke, Ding Weiwei, Yu Zhiteng. 2025. A new fixed-depth suspension control algorithm for mobile marine seismometer and its testing results. Acta Oceanologica Sinica, 44(2): 91–103, doi: 10.1007/s13131-024-2422-8

1 Introduction

Seismology was developed as a discipline in the 1889 and has since become an essential method for studying various aspects of earth's structure and geology, and it is based on a variety of data acquired by seismometers installed at seismic stations (Ben-Menahem, 1995). Thousands of permanent seismic stations have been operated on continental landmasses and islands, but few stations are located in the ocean, which covers nearly two-thirds of the area of the planet. This substantially restricts our understanding of the deep structure of the earth under the oceans. Ocean-bottom seismometers (OBSs) are helpful instruments for collecting seismic data in the sea. However, OBSs are typically deployed for no more than one year due to their limited battery capacity. Furthermore, the high cost of delivery and recovery of OBSs also restricts their long-term uses, resulting in a significant lack of off-

Foundation item: The National Key Research and Development Program of China under contract Nos. 2021YFC3101401 and 2022YFC3003802; the Deep Blue Fund under contract No. SL2103; the Zhejiang Provincial Key Research and Development Program under contract No. 2021C03186; the Zhejiang Provincial Natural Science Foundation of China under contract No. LDQ24D060001; the Open Fund Project of Key Laboratory of Ocean Observation Technology, MNR under contract No. 2024klootA11.
*Corresponding author, E-mail: jbli@sio.org.cn

shore seismic observation coverage, which has limited large/global-scale tectonic and structural studies (Tolstoy et al., 2006).

To overcome the problems mentioned above, the development of floating ocean seismometers started in late 1980 (Joubert et al., 2015, 2016; Simon et al., 2021; Simons, 2021; Simons et al., 2009; Sukhovich et al., 2015), of which the typical representative is the mobile marine seismograph (MMS), a vertical underwater vehicle. Compared to traditional fixed land-based seismic stations and OBSs, the MMSs can be suspended at a fixed depth, move with ocean currents, and transmit data via satellites, reducing the cost of seismic data recovery. MMSs can record signals conveyed by earthquakes (seismic P-waves) and thus are used to establish a seismic network covering an extensive marine area, solving the lack of long-term seismic stations in the oceans. In addition, the design lifespan of MMS exceeds three years, enabling the acquisition of additional seismic data, and is especially suitable for seismic tomography over large marine areas.

One of the critical operational requirements for an MMS is that it remains suspended at a desired depth for seismic monitoring for a specified time. Usually, the desired depth is around 1 500 m, below the axial depth of the deep ocean sound channel (SOFAR), around 1 000 m (Liang et al., 2020; Xu et al., 2023) (Fig. 1). This depth requirement aims to reduce the probability of the MMS from detecting the T-wave signal that propagates in the surface acoustic channel and then reduce the likelihood of false triggering of the seismic signal identification algorithm (Simon et al., 2021). This depth requirement also allows the MMS to achieve whole-ocean operation due to its lower resistance to pressure compared with other types of marine seismometers, which reduces the complexity of equipment design. Therefore, constant-depth control of MMSs is crucial.

The array for real-time geostrophic oceanography (ARGO) buoy is another representative of the floating ocean instruments, and it has been widely deployed in the ocean. An ARGO buoy could measure seawater density using its onboard conductivity-temperature-depth (CTD) sensor to calculate the displacement volume required to hover at different depths. This capability enables rapid and precise fixed-depth hovering. However, this method for achieving constant depth hovering is unavailable due to the absence of a CTD sensor on MMS. Currently, research on the control technology of ocean observation equipment is based primarily on the proportional-integral-derivative (PID) algorithm and its various improvements (Carneiro et al., 2023; Hu et al., 2022; Huang et al., 2020; Keow et al., 2020; Ranganathan et al., 2020; Sholl et al., 2022). However, unlike autonomous underwater vehicles (AUVs), remotely operated vehicles (ROVs), and manned submersibles, most deep-sea self-powered MMSs are not equipped with peripheral feedback actuators such as thrusters, resulting in slow buoyancy change and vertical motion of the MMS (Gigacz et al., 2018; Poksawat et al., 2018; Sholl et al., 2022).

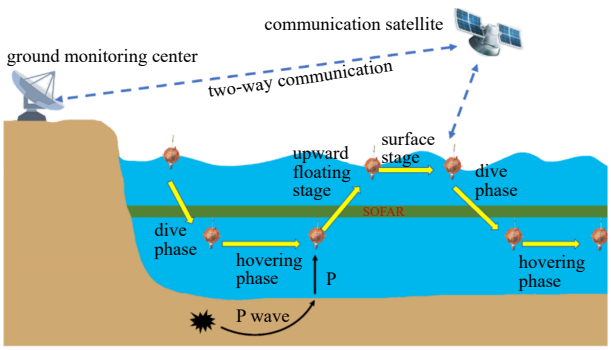

Fig. 1. Schematic diagram of the operation of an MMS.

For the profile buoy, like an MMS that achieves vertical motion by changing buoyancy for ascent and descent, the system's inertia affects the vertical movement of the float, resulting in a delayed response in the control process. Many studies have been extensively conducted on the fixed-depth control issues of such autonomous profiling floats. Barker (2014) proposed a closed-loop control method that linearized a nonlinear model for a buoy depth-fixing control problem. However, in their study, oscillatory motion was observed when the float velocity was near zero, the motor restarted frequently, and the energy consumption for depth control was high, indicating that the equipment was unsuitable for long-term operation. Therefore, using conventional control methods like PID to control the self-sustaining profiling buoy will lead to a significant overshoot, steady-state system error, and frequent oil-pump motor action (Shi and Chad, 2014). In response to these problems, various depth control algorithms have been proposed (Wang et al., 2022; Qiu et al., 2020; Zhang et al., 2020). Although the advanced algorithms exhibit delayed response and anti-interference capabilities, the model construction is complex, and the execution cost is high. In addition, these methods did not provide specific experimental validation, and the reliability and stability need further verification.

The MMS is a self-disposing device that carries limited onboard battery energy and must achieve a balance between the depth fixing and the cost of execution when executing fixed-depth suspension control. This study proposes a method of depth control for an MMS that addresses the issues of frequent buoyancy adjustments and high power consumption associated with PID and other control methods. The proposed method features fast convergence and efficient memory control, designed for fixed-depth adjustment while considering the constraints of inertia, delayed response, and limited battery energy.

2 Force analysis

An MMS consists of a protective case, a pressure-resistant compartment, an antenna, a hydrophone, a battery,

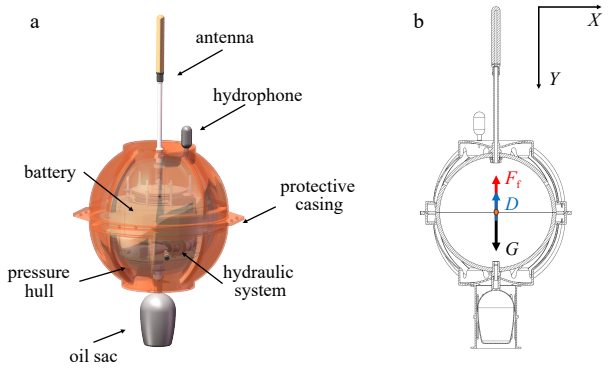

Fig. 2. Seismometer structure (a) and seismometer force analysis (b).

and a buoyancy-adjustment mechanism (Fig. 2a). The buoyancy-adjustment mechanism adjusts the net buoyancy of the MMS by changing the oil volume of the internal and external oil bladders, thereby controlling the ascent and descent of the MMS. During the descending stage, the MMS must overcome seawater density variations, dive to the preset operating depth, and adjust its net buoyancy through the fixed-depth suspension algorithm.

Force analysis of the MMS is required to intuitively analyze the vertical motion of an MMS during diving, suspension, and surfacing. A two-dimensional coordinate system is established with the depth measured in the vertical dimension as the coordinate Y-axis positive direction and any direction parallel to the sea surface as the X-axis positive direction. This study ignores the influence of the vertical component of the current on the motion of the MMS and the effect of seawater pressure on its shape change in order to simplify the state of motion analysis of the MMS. Because the pressure hull is made of glass material and has a slight deformation, the size of the MMS itself relative to its ascent and descent motion varies only very slightly, and the effect of the volume change can be ignored. The MMS is then subjected to the joint action of gravity (G), buoyancy (F_f), and resistance (D) during ascent and descent, as presented below. A simplified schematic of the MMS is shown in Fig. 2b.

(1) Gravity: The MMS is subjected to gravity (G) according to the expression

$$G = m \cdot g, \tag{1}$$

where m is the total mass of the MMS and g is the acceleration due to gravity.

(2) Buoyancy: The buoyancy force (F_f) on an MMS in seawater is equal to its weight when discharging seawater vertically upward and can be expressed as

$$F_f = -\rho(h) \cdot g \cdot V = -\rho(h) \cdot g \cdot (V_0 + V(\tau)), \tag{2}$$

where $\rho(h)$ is the density of seawater at a depth of h; V is the drainage volume of the MMS; V_0 is the initial drainage volume (without the external oil bladder) of the MMS, and $V(\tau)$ is the volume of the external oil bladder.

(3) Resistance: Assuming that the MMS has a smooth form, its free fall in static seawater is subject to total resistance (D), expressed as (Tian et al., 2021)

$$D = -\frac{1}{2}\rho(h) C_D v^2 A, \tag{3}$$

where C_D is the drag coefficient, v is the ascent and descent speeds of the MMS, and A is the cross-sectional area of the MMS.

The combined forces of gravity determine the ascent and descent acceleration of the MMS, buoyancy, and drag as follows:

$$\sum F = G + F_f + D = m \cdot a, \tag{4}$$

where $\sum F$ is the combined forces of gravity, buoyancy, and resistance, and a is the acceleration of the MMS.

When the MMS floats on the sea surface, the vertical direction of motion speed $v = 0$ according to Eq. (3). The MMS is subject to resistance $D = 0$ according to Eq. (4), and gravity G and buoyancy F_f are equal in strength and opposite in direction, meaning that the MMS is in equilibrium of forces. When the MMS starts to dive, the buoyancy-adjustment system transfers hydraulic oil from the outer bladder to the inner bladder, resulting in a smaller volume of the outer bladder; i.e., $V(\tau)$ decreases, which causes gravity acting on the MMS to be greater than the buoyancy force provided by the seawater. According to Eq. (4), the MMS is subjected to a combined force more significant than 0 and increases speed during its dive. As the dive depth increases, the density of seawater increases, and according to Eq. (2), the buoyancy force provided by seawater increases, and the MMS starts to decelerate; without changing the volume of the MMS, the MMS reenters force equilibrium, that is, $\sum F = 0$, where $D = 0$ and $v = 0$. According to Eqs (1), (2), and (4),

$$\rho(h) \cdot g \cdot (V_0 + V(\tau)) = m \cdot g. \tag{5}$$

Which gives

$$V(\tau) = \frac{m}{\rho(h)} - V_0. \tag{6}$$

According to the high-pressure equation of state for seawater, the seawater density equation is obtained from the temperature, salinity, and pressure as follows:

$$\rho(S, T, P) = \frac{\rho(S, T, 0)}{1 - \dfrac{P}{K(S, T, p)}}, \tag{7}$$

$$\rho(S, T, 0) = \rho_W + A_1 S + A_2 S^{\frac{3}{2}} + A_3 S^2, \tag{8}$$

where $\rho(S, T, P)$, $K(S, T, P)$, and $\rho(S, T, 0)$ denote the seawa-

ter density at high pressure, typical bulk modulus, and seawater density at standard atmospheric pressure, respectively; P, T, and S denote the pressure, temperature, and salinity, respectively; and A_1, A_2, and A_3 are coefficients related to the properties of seawater. The units and values of the variables used in these equations are listed in Table 1.

3 Neutral buoyancy search for the fixed-depth control method

As derived in Section 2, seawater density and seawater pressure are one-to-one mapping functions. Considering that seawater pressure also corresponds uniquely to seawater depth h, seawater density at different depths also corresponds uniquely to seawater depth. Then, it is known that MMSs with varying volumes of drainage will be suspended at different seawater densities related to seawater depth without considering the influence of currents.

The algorithm's core is to employ a binary search method to quickly and accurately determine the appropriate displacement volume based on the seismometer's depth and vertical velocity, thereby enabling fixed-depth hovering. The device relies solely on buoyancy changes for vertical movement, which leads to a significant time delay in the control system. This study analyzes the motion trends of the seismometer and establishes two boundary conditions for buoyancy control to prevent excessive adjustments that could result in oscillations and increased energy consumption.

Once fixed-depth hovering is achieved, the algorithm records the current buoyancy value to reference future depth control. Given that the device's drift distance during a single operational cycle is limited and seawater density remains relatively stable, utilizing this reference value reduces the number of buoyancy adjustments required. This approach facilitates faster depth stabilization, lowers energy consumption, and extends the device's lifespan.

3.1 *Principles of fixed-depth control*

Suppose that the real-time depth of the MMS is d, the set suspension depth is H, the allowable depth fluctuation during suspension is ΔH, the drainage volume is V, and the buoyancy interval required for being suspended at depth $(H-\Delta H, H+\Delta H)$ is $(F_{H+\Delta H}, F_{H-\Delta H})$. A seawater pressure gauge determined the real-time depth. According to Eq. (6), it is known that the buoyancy force $F(V)$ of the MMS is continuous over the interval $(V_{\min}, V_{\max})$ where $V_{\max}$ is the maximum drainage volume and $V_{\min}$ is the minimum drainage volume. When $F(V_{\min}) < F_{H+\Delta H}$, $F(V_{\max}) > F_{H-\Delta H}$, where $F(V_{\min})$, $F(V_{\max})$ are the equipment-adjustable maximum buoyancy and minimum buoyancy, respectively, then there must exist $V_{\text{hover}} \in (V\_\min, V\_\max)$ so that $F(V_{\text{hover}}) \in (F_{H+\Delta H}, F_{H-\Delta H})$, for which the MMS achieves constant-depth suspension (Fig. 3).

Therefore, when the buoyancy control system starts to find V_{hover} from $V_{\min}$, if there is $F(V_a) - F_{H-\Delta H} < 0$ and $F(V_b) - F_{H+\Delta H} > 0$, then there must be $V_{\text{hover}} \in (V\_\min, V\_\max) \in (V_a, V_b)$; i.e., $F(V_{\text{hover}}) \in (F(V_a), F(V_b))$, where V_a, V_b is the MMS drainage volume adjustment interval and $F(V_a)$, $F(V_b)$ is the corresponding buoyancy.

3.2 *Fixed-depth control algorithm adjustment mechanism*

Because the changes in the buoyancy and vertical motion of the MMS are slow and influenced by the inertia of the system, a response time lag exists in the control process. Therefore, to improve the control effect, it is necessary to analyze the fluctuation in the vertical motion of the MMS to avoid an invalid buoyancy adjustment. As shown in Fig. 4, even if the MMS exceeds the upper and lower boundaries of the fixed-depth range for a short time, it is feasible to complete the fixed-depth suspension gradually. Therefore, the relationship between d and H, and ΔH cannot be simply used as the basis for buoyancy regulation. The analysis revealed two cases that required immediate buoyancy adjustment: beyond the upper boundary and with a tendency to ascend or suspend, and beyond the lower boundary and with a tendency to sink or suspend. In the case of the remaining motion states, it is only necessary to wait for the MMS depth to change until it reaches one of the above two states or achieves a suspension.

In the process of controlling the MMS to suspend at a fixed depth, if the effect of the vertical component of the current motion is not considered when the buoyancy of

Table 1. The significant parameters in the calculation

Symbol	Value	Physical significance	Symbol	Unit	Physical significance
G	514.515 N	the gravity force	F_f	N	the buoyancy force
m	52.235 kg	the total mass of the MMS	D	N	the resistance force
g	9.85 m/s^2	the acceleration due to gravity	v	m/s	the ascent and descent speeds of the MMS
V	0.050 364−0.051 364 m^3	the volume of the external oil bladder	$\rho(h)$	kg/m^3	the density of seawater at a depth of h (m);
A	0.163 m^2	the cross-sectional area of the MMS	P	Pa	seawater pressure
V_0	0.049 164 815 m^3	the initial drainage volume of the MMS	T	℃	temperature
$V(\tau)$	1 200−2 200 cm^3	the volume of the external oil bladder	S		salinity
			a	m/s^2	the acceleration of the MMS

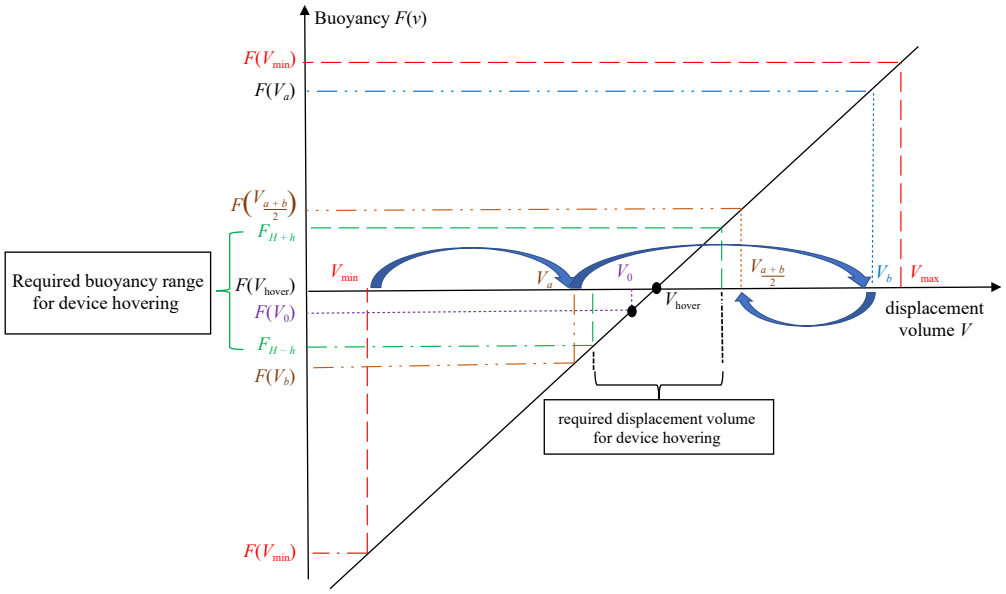

Fig. 3. Relationship between displacement volume and buoyancy for a mobile marine seismometer.

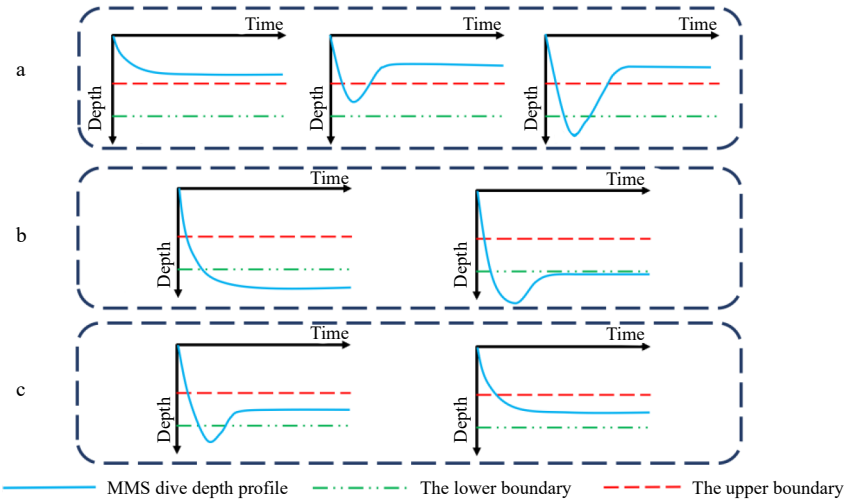

Fig. 4. MMS movement trends. a. The initial state of the MMS moves downward over the upper boundary but eventually hovers above it. b. The initial state of the MMS moves down over the lower boundary but eventually hovers below it. c. MMS attains fixed-depth hovering.

the MMS is adjusted to the suspension buoyancy interval $(F_{H+\Delta H}, F_{H-\Delta H})$, suspension can be realized in the depth interval $(H-\Delta H, H+\Delta H)$. In contrast, when the buoyancy of the MMS is not within the buoyancy interval $(F_{H+\Delta H}, F_{H-\Delta H})$, then this will undoubtedly trigger the condition for the two possible adjustments mentioned above. An adjustment of buoyancy will be required to correct the motion of the MMS. The principles of buoyancy regulation are presented below and in Fig. 5.

(1) Fixed step to find a fixed-depth buoyancy interval

Before the first k buoyancy adjustments are completed, the vertical motion trend of the MMS remains unchanged (Fig. 5), meaning that the buoyancy of the MMS always has $F > F_{H-\Delta H}$, and each oil adjustment is fixed $q_{k-1} = \cdots = q_k = q$.

(2) Determine the fixed-depth buoyancy interval

When the kth buoyancy adjustment is completed ($q_k = q_{k-1}$), the motion trend of the MMS changes, and the previous adjustment condition is not satisfied. The MMS may then appear in two states: gradually entering the suspension depth interval to achieve a constant-depth suspension, which satisfies $F \in (F_{k+1}, F_k)$; alternatively, if the MMS triggers another adjustment condition (e.g., the MMS lies beyond the lower boundary and has a sinking or suspending tendency), then $(F_{H+\Delta H}, F_{H-\Delta H}) \in (F_{k+1}, F_k)$ is satisfied, and the adjustment needs to be continued so that $F \in (F_{k+1}, F_k)$.

(3) Rapid convergence into a constant-depth buoyancy interval

To quickly converge the buoyancy of the MMS into $(F_{H+\Delta H}, F_{H-\Delta H})$ and achieve the effect of a constant-depth suspension within the depth layer $(H-\Delta H, H+\Delta H)$, the

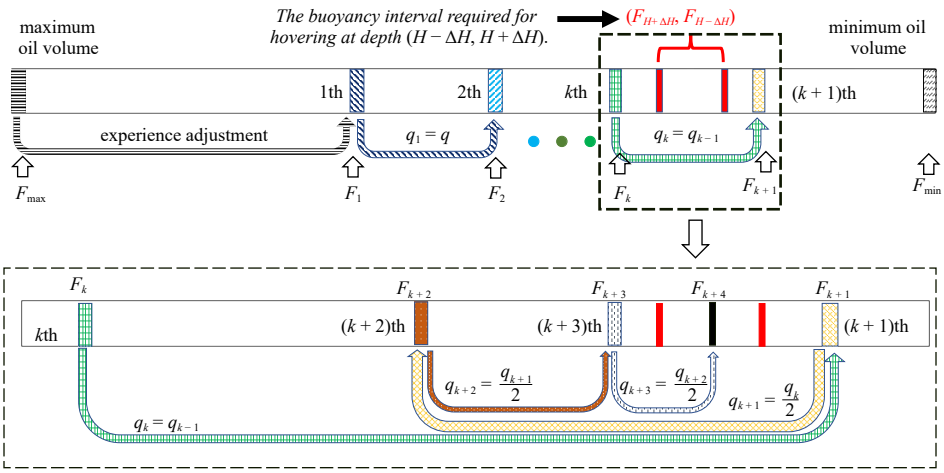

Fig. 5. Principles of buoyancy adjustment. The seismometer gradually reduces its displacement until it reaches the required volume for hovering.

principle of dichotomous zero-point calculation was adopted for buoyancy regulation. The oil volume adjustment after the first $(k+1)$ time is halved, that is, $q_{k+1}=\frac{q_k}{2}$, until $F\in(F_{k+1}, F_k)$, at which time the position of the MMS is stabilized, and the MMS is suspended within the depth $(H-\Delta H, H+\Delta H)$ with the set speed of ascent or descent.

3.3 *Fixed-depth control process*

The MMS adjusts its negative buoyancy to its maximum value at the beginning of the dive to achieve the highest speed. When the MMS dives to the upper boundary of the preset suspension depth range [i.e., $d=(H-\Delta H)$], it adjusts its buoyancy according to the neutral buoyancy of the previous suspension state; if the MMS is diving for the first time, its buoyancy will be adjusted based on the empirical value of seawater density. The purpose of this adjustment is to quickly bring the MMS to a neutral buoyancy state for suspension. It helps reduce the number of buoyancy corrections needed to maintain a fixed depth and prevents repeated adjustments. As a result, it lowers power consumption and shortens the adjustment time. In addition, after a completed duty cycle (usually seven days), the MMS moves a short distance with the current, the ocean environment does not change significantly, and the buoyancy state required for the suspension is similar. Referring to the previous suspension state can considerably reduce the number of buoyancy necessary adjustments to fix the depth, realize suspension rapidly, and reduce power consumption.

After completing the initial buoyancy adjustment, if the MMS is suspended within the preset operational depth range and shows fluctuation in depth at a speed less than the preset value, the MMS is considered to be in a suspended state; however, if the MMS exceeds the operational depth range and triggers the buoyancy adjustment condition, it is adjusted according to the neutral buoyancy adjustment mechanism in Fig. 6 until it meets the suspended state. After entering the suspended state, the MMS detects its depth change at a fixed frequency (usually set to 10 min); if the adjustment condition is triggered, it is adjusted according to the adjustment scheme shown in Fig. 6 to ensure that the MMS retains the suspended state. The pseudocode for the algorithm execution is shown in Table 2.

3.4 *Analysis of algorithm convergence speed and fixed-depth accuracy*

To achieve a fast and accurate determination of the required displacement volume for hovering, a method similar to the "bisection method" for root finding was employed. The displacement volume range was gradually narrowed until it approached the value of V_{hover}. Considering the midpoint of $[V_a, V_b]$, $V_0=\frac{1}{2}(V_a+V_b)$ and dividing the interval into two; if $F(V_0)-F_{H-\Delta H}>0$ and $F(V_0)-F_{H+\Delta H}<0$, then $V_0\in(V_{H+\Delta H}, V_{H-\Delta H})$ (where $(V_{H+\Delta H}, V_{H-\Delta H})$ is the drainage volume needed to reach neutral buoyancy at the depth $(H-\Delta H, H+\Delta H)$ of the device), and at this time, the MMS achieves constant-depth suspension. Otherwise, it is necessary to determine whether the interval $(V_{H+\Delta H}, V_{H-\Delta H})$ is to the left or right of V_0. If $(F(V_a)-F_{H-\Delta H})\times(F(V_0)-F_{H+\Delta H})<0$, then we have $(V_{H+\Delta H}, V_{H-\Delta H})\in(V_a, V_0)$ such that $V_{a1}=\mathrm{a}$, $V_{b1}=V_0$.

If $(F(V_0)-F_{H-\Delta H})\times(F(V_b)-F_{H+\Delta H})<0$, then $(V_{H+\Delta H}, V_{H-\Delta H})\in(V_0, b)$, such that $V_{a1}=V_0$, $V_{b1}=b(V_{a1}, V_{b1})$ is the new interval where neutral buoyancy exists, and its length is only half of the original interval, meaning that the aim of compressing the interval is achieved. By performing the operation mentioned above repeatedly, there is always $(V_{an}, V_{bn})\in(V_{a1}, V_{b1})$, and the length of the interval (V_{an}, V_{bn}) is $V_{bn}-V_{an}=\frac{1}{2^n}(V_a, V_b)$ (where n is the number of adjustments of buoyancy), then for a sufficiently large value of n, there must be $V_{hover}\in(V_{an}, V_{bn})\in(V_{H+\Delta H}, V_{H-\Delta H})$ to achieve fixed-depth suspension. The convergence rate of the algorithm is $V_{bn}=V_{an}+O\left(\frac{1}{2^n}\right)$.

The convergence speed of the fixed-depth algorithm

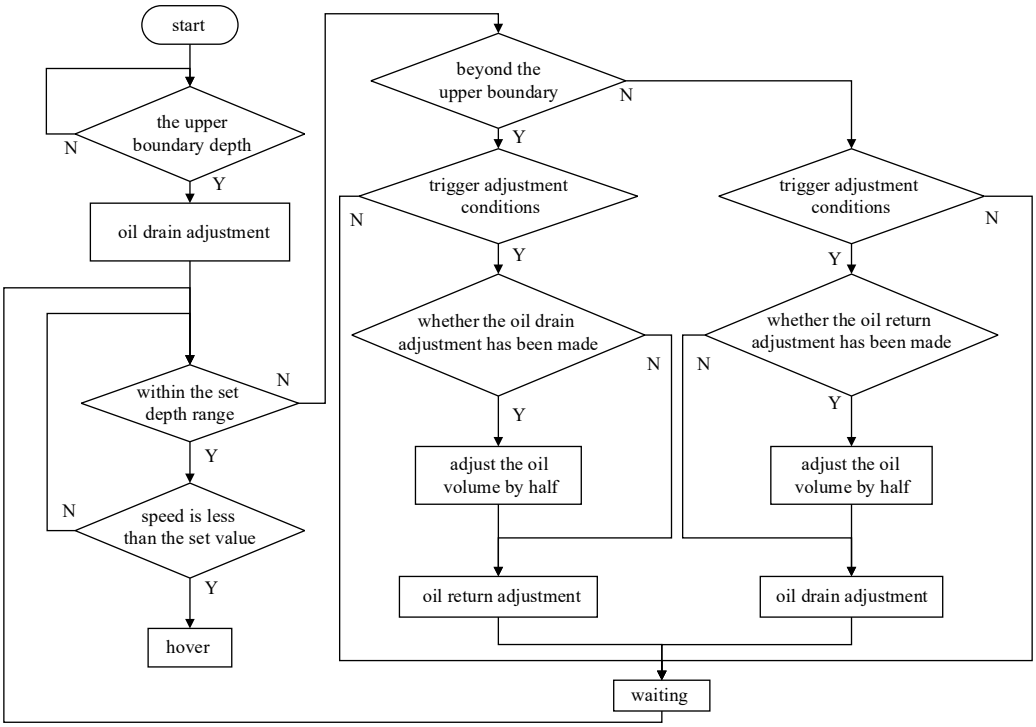

Fig. 6. Fixed-depth control process.

Table 2. Pseudocode for the algorithm

Input: the real-time depth of the MMS is d, the suspension depth is H, the allowable depth fluctuation during the suspension is ΔH, the previous suspension state V_p, the first k buoyancy adjustment q_k
Output: displacement volume V

```
1. V = V_p
2. if d < (H − ΔH) && Trigger adjustment
3. {
4. if Determination(q_k) { //whether the oil drain adjustment
5. q_k = q_k/2}
6. V = V − q_k
7. } else if d > (H +ΔH) && Trigger adjustment
8. {
9. if Determination(q_k) { //whether the oil return adjustment
10. q_k = q_k/2}
11. V = V + q_k
12.}
13. else {
If speed < the set value
14. hover
15.}
```

was influenced by variations in the seawater density, target fixed-depth value, range of fixed-depth control, and adjustment of oil quantity. Using actual measured seawater density data from the South China Sea (Fig. 7), we analyzed the convergence speed of the fixed-depth control algorithm. Assuming a target fixed depth of 1 000 m with an allowable deviation of ±50 m. By analyzing the number of times the control algorithm finds the appropriate neutral buoyancy range for different adjustment step sizes (q equal 0 mL to 100 mL), we consider the initial adjustment of the device at different neutral buoyancy states (after the initial adjustment, the device may hover at any depth owing to a lack of experience, leading to significant errors). The seawater density curve was approximated using segmented fitting to facilitate the simulation. When the seawater depth satisfies $400\ \text{m} \leqslant d \leqslant 1\ 800\ \text{m}$, the relationship between the seawater density ρ and depth d can be described using a cubic curve with the following equation:

$$\rho(d) = 4.581 \times 10^{-10} d^3 - 2.410\ 5 \times 10^{-6} d^2 + 0.008\ 947\ 9d + 1\ 025.028\ 5. \quad (9)$$

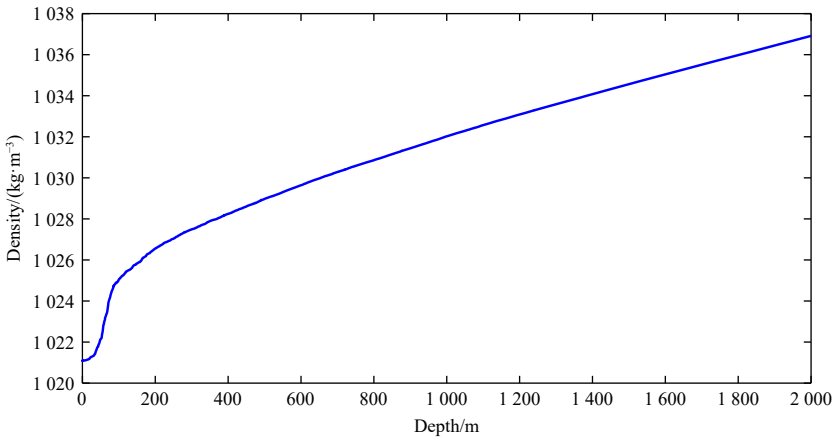

Fig. 7. Seawater density data for the South China Sea.

The simulation results are shown in Fig. 8. Point A represents the scenario in which, after the initial buoyancy adjustment, the device can hover at a depth of 989 m with zero adjustment iterations, achieving the desired hovering state. Point B represents the scenario in which, after the initial buoyancy adjustment, the device can hover at a depth of 800 m, requiring three adjustment iterations for the control algorithm to achieve the necessary buoyancy for hovering. The simulation results indicated that the number of adjustment iterations decreased as the adjustment step size increased. However, larger adjustment step sizes result in longer pump activation, leading to energy wastage. When the adjustment step size exceeded 20 mL, a further increase in the step size did not significantly reduce the number of adjustment iterations. Therefore, a step size of 20 mL was used in this study. Even with more significant errors (500 m), hovering was achieved through six adjustment iterations. The analysis demonstrated that the algorithm has a theoretically fast convergence speed when selecting an appropriate adjustment for the oil volume.

According to Eqs (6), (7), and (9), a one-to-one mapping relationship exists between the displacement volume of the mobile marine seismometer and the depth of the hover. The relationship between the displacement volume $(V_0 + V(\tau))$ and hover depth H is expressed as follows:

$$\frac{m}{V_0 + V(\tau)} = 4.581 \times 10^{-10} H^3 - 2.410\,5 \times 10^{-6} H^2 + 0.008\,947\,9H + 1\,025.028\,5, \quad (10)$$

where m represents the total mass of the seismometer, V_0 represents the initial displacement volume of the seismometer (excluding that of the external oil bladder), $V(\tau)$ represents the volume of the external oil bladder, and H represents the depth at which the seismometer hovers ($400\ \text{m} \leqslant H \leqslant 1\,800\ \text{m}$). The minimum adjustment in the displacement volume of the device determined the accuracy of the fixed-depth suspension. Based on the relationship between the displacement volume and the hover depth in Eq. (10) and considering the displacement volume at the target hover depth of 1 000 m as a reference, the variation in the displacement volume (ΔV) concerning the hover depth is plotted as shown in Fig. 9. The algorithm controls the oil volume by regulating the opening time of the plunger pump and using potentiometer feed-

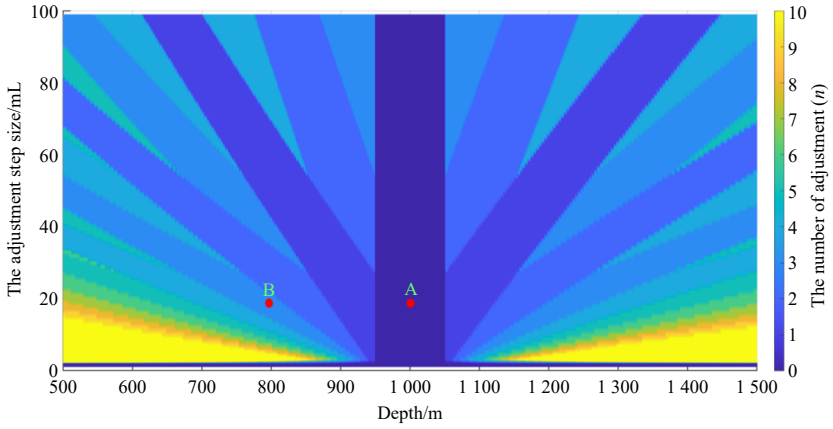

Fig. 8. Number of adjustments of the fixed-depth algorithm concerning oil volume. Here, *X*-axis represents the depth (m) at which hovering is possible after the initial buoyancy adjustment, *Y*-axis represents the adjustment step size of the displacement volume (mL) for each iteration, and color bar represents the number of adjustments required to achieve the neutral buoyancy necessary for hovering.

back to detect the oil bladder position. Actual oil volume control was achieved with a precision of 2 cm^3, resulting in a depth-control accuracy of 7.5 m.

4 MMS sea trial and results

A sea trial of the MMSs was conducted in the South China Sea starting in April 2021. The trial was executed in a sea area with a radius of 50 n mile centered on 17°46.9′N, 114°24.1′E, and the average water depth of the trial area was greater than 2 000 m, meeting the water-depth requirements (Fig. 10a). The sea trial was conducted in two phases. The first stage was a short-term trial of nine MMSs to verify the implementation process and the effect of the depth control algorithm (Fig. 10b). The second stage was a long-term trial of two MMSs to verify their operation under natural oceanic operating conditions (Fig. 10c).

4.1 *Short-term trial*

The short-term trial (Fig. 10b) parameters were set as follows: a suspension depth fixed at 1 000 m, an allowable vertical fluctuation range of ±50 m, an entry of the MMS into the suspension state when the rising and sinking speed is less than 0.01 m/s and an initial adjustment of oil volume of 10 mL. The execution of the fixed-depth

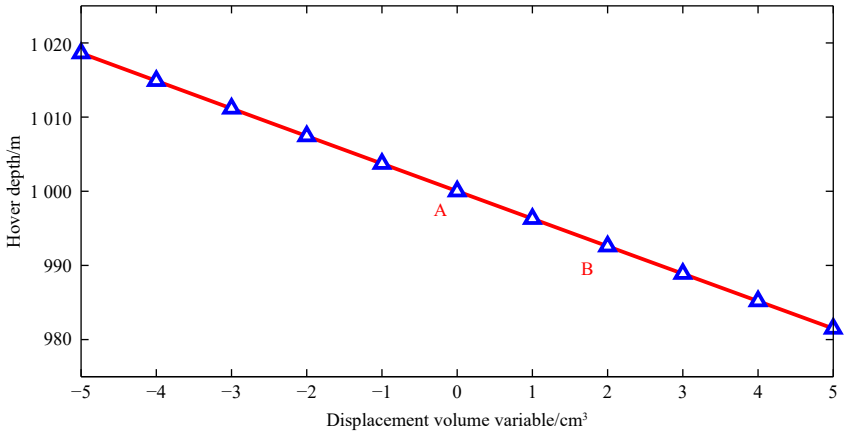

Fig. 9. The relationship between the variation in displacement volume (with the displacement volume at 1 000 m hover depth as the reference).

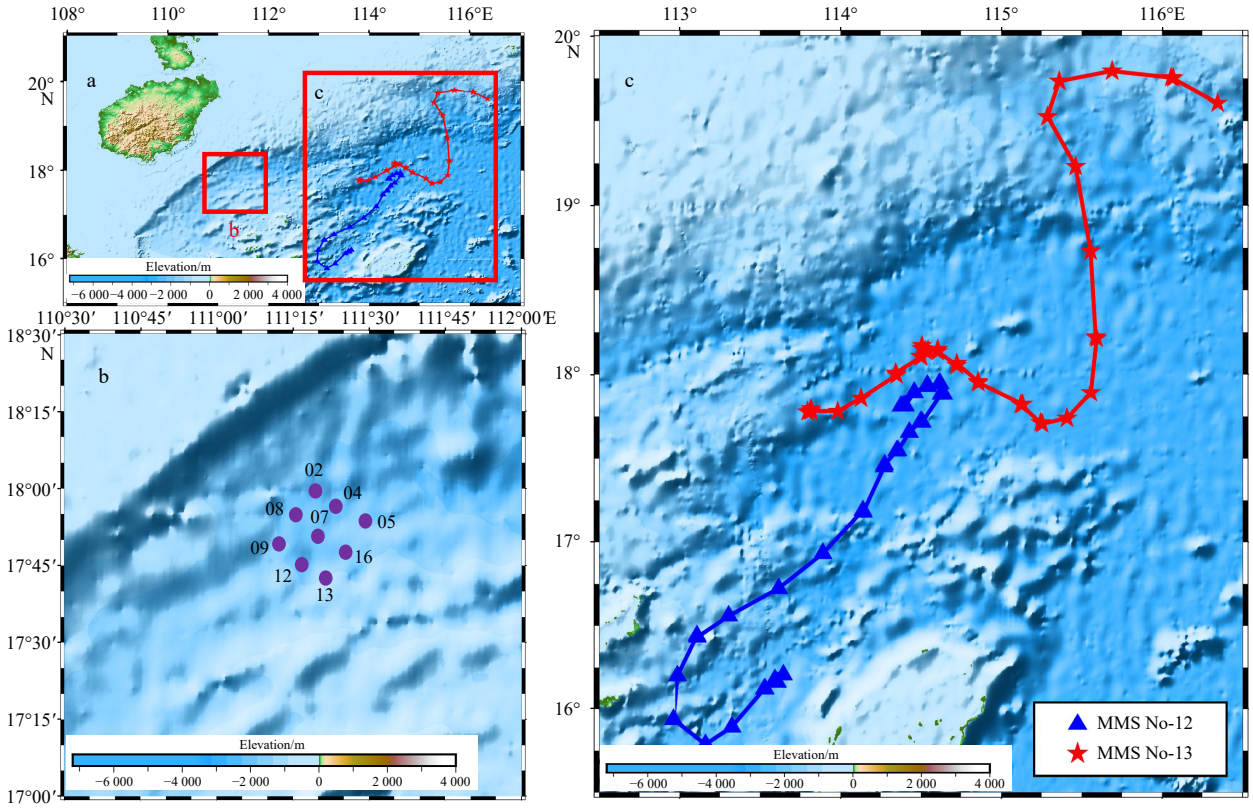

Fig. 10. Trial area and MMS drift tracks.

suspension algorithm is analyzed here using MMS No-9 as an example (Fig. 11), where the blue curve represents the depth profile of the MMS, and the two red dashed lines represent the upper and lower boundaries of the set constant depth interval, respectively. The MMS sank at speed (approximately 0.17 m/s) from the sea surface with maximum negative buoyancy. After falling to the upper boundary of the suspension zone, the first buoyancy adjustment was performed (the adjustment amount was calculated based on the seawater density in the adjacent sea measured by the Argo buoy). This buoyancy adjustment was completed when the MMS dived to a depth of 1 013.7 m. Subsequently, the MMS ascended slightly, exceeding the upper boundary of the suspension zone and triggering the buoyancy-adjustment condition. The MMS made four consecutive oil transfer adjustments to control its buoyancy to enter the fixed-depth suspension zone with a sinking speed of <0.01 m/s, thereby entering the suspension state. Four hours later, once the preset submersion time was reached, the MMS was adjusted to the maximum positive buoyancy state and returned to the sea surface.

The vertical profiles of the other MMSs involved in the short-term trial are presented in Fig. 12. MMS No-12 and No-16 were set to a fixed depth of 500 m, and the rest of the MMSs were set to a fixed depth of 1 000 m. The depth curves show that different seismometers can be suspended relatively quickly after a short adjustment period. The short-term trial shows that the fixed-depth control algorithm designed in this study could achieve an MMS fixed-depth suspension with fewer buoyancy adjustments (less than four times on average during the experiment) and better suspension control in the case of unknown seawater density.

4.2 *Long-term trial*

Based on the results of the short-term trial, the two MMSs were placed in the trial area for a 3-month-long applicability trial to verify their overall operating performance. The MMSs were recovered in early August 2021. During the trial period, the two MMSs were operated for 95 d, with 44 cycles and 532 n mile of travel. The MMSs were 258 n mile apart at the time of recovery. The drift tracks of the two MMSs are shown in Fig. 10c.

The parameters of this trial were set as follows: a suspension depth of 800 m, an allowable vertical fluctuation range of ±100 m, and an entry of the MMS into the sus-

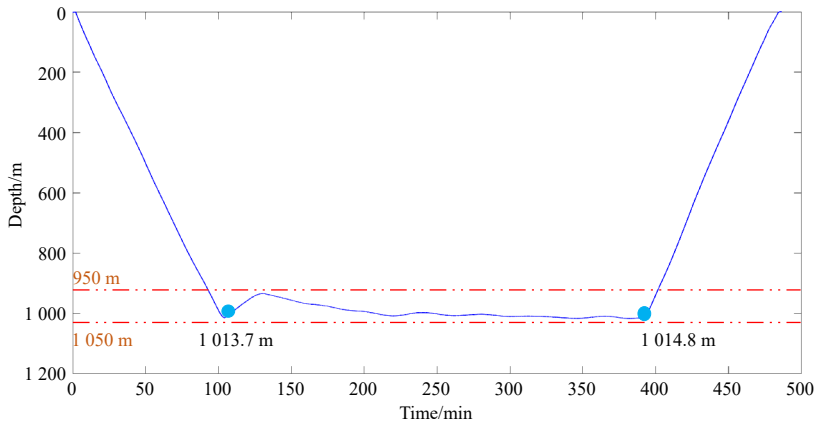

Fig. 11. The dive depth curve for the MMS No-9 and the two red dashed lines represent the upper and lower boundaries of the set constant depth interval, respectively.

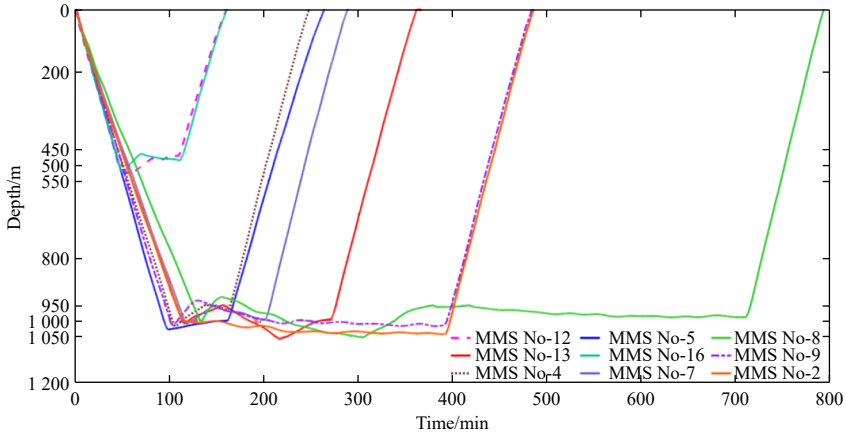

Fig. 12. The dive depth curve for MMSs, where MMS No-12 (purple dotted line) and No-16 (light blue) were set to a fixed depth of 500 m, and the rest of the MMSs were set to a fixed depth of 1 000 m.

pension state at a speed of <0.01 m/s. The dive duration of the MMSs gradually increased over time (Fig. 13a). The blue curve represents the operating time of MMS No-12 across various dive cycles. The first ten dives had shorter durations, averaging 55 h, while the last 12 dives were extended to 6.5 d. The red curve indicates the operating time of MMS No-13. An analysis of the operating status of the MMS for three months showed that the MMSs were in a fixed-depth suspension state 98% of the time (Fig. 13b), indicating that the fixed-depth control algorithm can realize MMS long-term fixed-depth suspension and reduce the influence of ocean currents, enabling the MMS to record seismic events.

As shown in Fig. 14a and Fig. 15a, as the number of MMS dives increased, the overall number of starts of the fixed-depth suspension control algorithm decreased. The average number of adjustments was reduced by about 10. At a depth of 800 m underwater, the energy consumption for a single buoyancy adjustment of the seismometer is 0.067 W·h, resulting in a total energy savings of 0.67 W·h per profile. Through semi-physical simulation testing, the device's power consumption for a single operational cycle (7 d) was 27 W·h, with an energy savings of 2.5%. Based on the device's designed lifespan of 3 years, the algorithm can save 105 W·h compared to the initial adjustment, extending the operational period by 3.9 cycles. Also, as shown in Figs 14b and 15b, the MMSs can achieve a satisfactory effect in long-term operations, with an average suspension depth of 765.4 m in the long-term trial and an average drift depth of 29.6 m. The long-term trial showed that the fixed-depth suspension algorithm designed in this study can effectively and efficiently control an MMS to achieve a fixed-depth suspension and that the maintenance of the position of the MMS within the suspension zone is also satisfactory.

5 Conclusions

In this study, we addressed the problem of fixed-depth suspension control for a mobile marine seismometer with

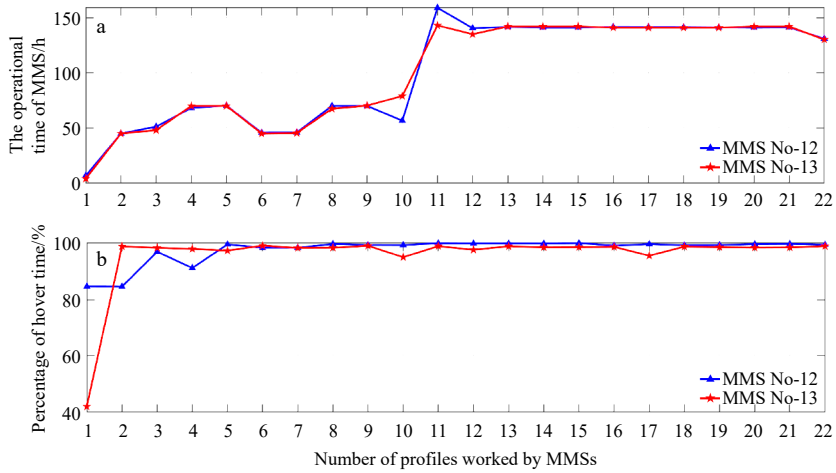

Fig. 13. MMS operating status. a. The operational time of MMS (h) of MMS duty cycles. b. Time in suspension at a fixed depth as a percentage of dive time for the MMS.

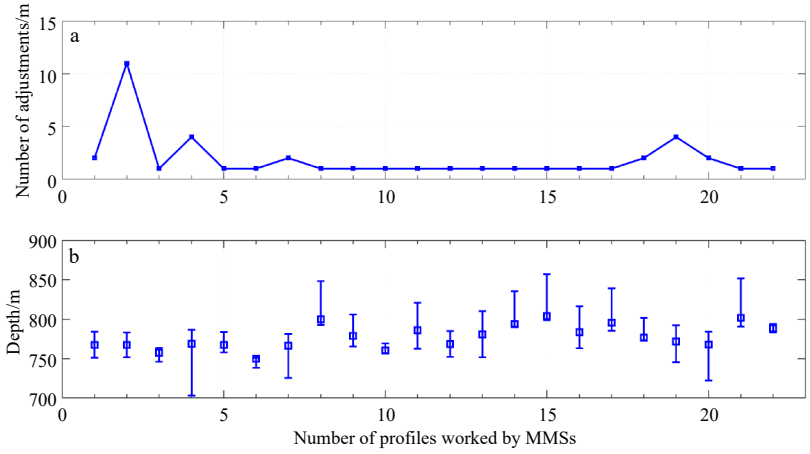

Fig. 14. Number of buoyancy adjustments needed to achieve fixed-depth suspension at different points along the drift tracks of the MMS No-12 (a) . Average suspension depth and error at different points along the drift tracks of the MMS No-12 (b).

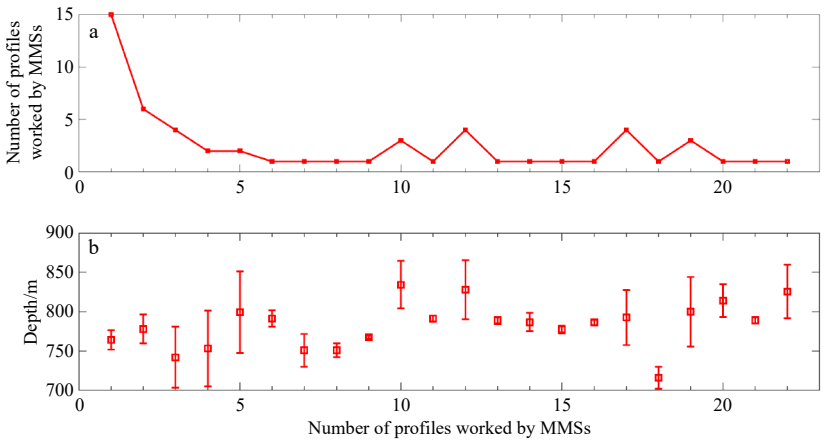

Fig. 15. Number of buoyancy adjustments needed to achieve fixed-depth suspension at different points along the drift tracks of the MMS No-13 (a). Average suspension depth and error at various points along the drift tracks of the MMS No-13 (b).

a limited onboard energy supply. We developed an effective fixed-depth control algorithm with a low depth adjustment cost that does not depend on seawater density data by establishing an MMS motion model and analyzing the fluctuations in vertical motion. Sea trials demonstrated that the control algorithm produced a satisfactory fixed-depth suspension, maintained the desired fixed depth, and mitigated the influence of ocean currents without requiring complex computations or hydrodynamic analysis of the MMS.

The algorithm's simplicity and low computational requirements make it suitable for drifting buoys like the MMS, which rely solely on buoyancy adjustments for vertical motion. This innovative approach provides a new avenue for the fixed-depth control of other deep-sea equipment that utilizes buoyancy adjustments via an oil bladder, enhancing performance without complex control systems. Additionally, the algorithm has a memory function that allows for faster subsequent depth adjustments, reducing the number of corrections, lowering energy consumption, and extending the operational lifespan of the equipment.

References

Barker L. 2014. Closed-loop buoyancy control for a coastal profiling float. MBARI Intern Rep, Moss Landing, CA, USA, 1–15

Ben-Menahem A. 1995. A concise history of mainstream seismology: origins, legacy, and perspectives. Bulletin of the Seismological Society of America, 85(4): 1202–1225

Carneiro J F, Pinto J B, de Almeida F G, et al. 2023. Model identification and control of a buoyancy change device. Actuators, 12(4): 180, doi: 10.3390/act12040180

Gigacz R, Mohamed A, Poksawat P, et al. 2018. Exploring tandem wing UAS designs for operation in turbulent urban environments. International Journal of Micro Air Vehicles, 10(3): 254–261, doi: 10.1177/1756829318794167

Hu Rui, Lu Di, Xiong Chengke, et al. 2022. Modeling, characterization and control of a piston-driven buoyancy system for a hybrid aerial underwater vehicle. Applied Ocean Research, 120: 102925, doi: 10.1016/j.apor.2021.102925

Huang Haocai, Zhang Chenyun, Ding Weiwei, et al. 2020. Design of the depth controller for a floating ocean seismograph. Journal of Marine Science and Engineering, 8(3): 166, doi: 10.3390/jmse8030166

Joubert C, Nolet G, Bonnieux S, et al. 2016. *P* - Delays from floating seismometers (MERMAID), part I: data processing. Seismological Research Letters, 87(1): 73–80, doi: 10.1785/0220150111

Joubert C, Nolet G, Sukhovich A, et al. 2015. Hydrophone calibration at very low frequencies. Bulletin of the Seismological Society of America, 105(3): 1797–1802, doi: 10.1785/0120140265

Keow A, Chen Zheng, Bart-Smith H. 2020. PIDA control of buoyancy device enabled by water electrolysis. IEEE/ASME Transactions on Mechatronics, 25(3): 1202–1210, doi: 10.1109/tmech.2020.2968322

Liang Qingwei, Ou Junlin, Xue Zengxi. 2020. All-terminal reliability of multi-AUV cooperative systems in horizontally stratified SOFAR channel. Ships and Offshore Structures, 15(5): 474–478, doi: 10.1080/17445302.2019.1661620

Poksawat P, Wang Liuping, Mohamed A. 2018. Gain scheduled attitude control of fixed-wing UAV with automatic controller tuning. IEEE Transactions on Control Systems Technology, 26(4): 1192–1203, doi: 10.1109/tcst.2017.2709274

Qiu Zurong, Wang Qiang, Yang Shaobo, et al. 2020. Depth control for a deep-sea self-holding intelligent buoy system based on active disturbance rejection control method. Journal of Measurement Science and Instrumentation, 11(4): 307–316

Ranganathan T, Singh V, Thondiyath A. 2020. Theoretical and experimental investigations on the design of a hybrid depth controller for a standalone variable buoyancy system-*vBuoy*. IEEE Journal of Oceanic Engineering, 45(2): 414–429, doi: 10.1109/joe.2018.2875576

Shi Xianpeng, Chad L. 2014. Research and application of the

depth control technology for a class of underwater autonomous drifting floats. Journal of Ocean Technology (in Chinese), 33(5): 13–17

Sholl N, Nelson K, Mohseni K. 2022. Autonomous underwater vehicle depth and pitch trajectory tracking using fiber-reinforced elastomer bladders for buoyancy control. IEEE Journal of Oceanic Engineering, 47(3): 690–703, doi: 10.1109/joe.2021.3128676

Simon J D, Simons F J, Irving J C E. 2021. A MERMAID miscellany: seismoacoustic signals beyond the *P* wave. Seismological Research Letters, 92(6): 3657–3667, doi: 10.1785/0220210052

Simons F J. 2021. Twenty-thousand leagues under the sea-recording earthquakes with autonomous floats – Frederik J. Simons, Joel D. Simon, and sirawich pipatprathanporn. Acoustics Today, 17(2): 42, doi: 10.1121/at.2021.17.2.42

Simons F J, Nolet G, Georgief P, et al. 2009. On the potential of recording earthquakes for global seismic tomography by low-cost autonomous instruments in the oceans. Journal of Geophysical Research: Solid Earth, 114(B5): B05307, doi: 10.1029/2008jb006088

Sukhovich A, Bonnieux S, Hello Y, et al. 2015. Seismic monitoring in the oceans by autonomous floats. Nature Communications, 6: 8027, doi: 10.1038/ncomms9027

Tian Xin, Zhang Hongwei, Zhang Lianhong, et al. 2021. Research on positive buoyancy underwater glider and its sailing efficiency. Applied Ocean Research, 110: 102592, doi: 10.1016/j.apor.2021.102592

Tolstoy M, Cowen J P, Baker E T, et al. 2006. A sea-floor spreading event captured by seismometers. Science, 314(5807): 1920–1922, doi: 10.1126/science.1133950

Wang Qiang, Li Xingfei, Qiu Zurong, et al. 2022. Depth-keeping control for a deep-sea self-holding intelligent buoy system based on inversion time constraint stability strategy optimization. Sensors, 22(3): 1096, doi: 10.3390/s22031096

Xu Jiajie, Kishk M A, Zhang Qunfei, et al. 2023. Three-hop underwater wireless communications: a novel relay deployment technique. IEEE Internet of Things Journal, 10(15): 13354–13369, doi: 10.1109/jiot.2023.3262949

Zhang Bowei, Li Xingfei, Li Hongyu, et al. 2020. Depth control of deep-sea profiling float based on ADRC. Transducer and Microsystem Technologies (in Chinese), 39(10): 100–103, doi: 10.13873/J.1000-9787(2020)10-0100-04